Received: December 16, 2023. Revised: January 9, 2024. 464

International Journal of
Intelligent Engineering & Systems

http://www.inass.org/

Fused Feature Vector and Dual FCM for Lung segmentation from Chest X-Ray Images

Duvva Naresh Kumar[1]* **M. Kezia Joseph[2]**

[1]*Department of Electronics and Communication Engineering, Osmania University, Hyderabad, Telangana, India*
[2]*Department of Electronics and Communication Engineering,*
Stanley College of Engineering and Technology for Women, Hyderabad, Telangana, India
* Corresponding author's Email: duvvanaresh@gmail.com

Abstract: Segmentation of Lung Region is an important step in the clinical diagnosis of lung diseases like Pneumonia, Tuberculosis, and COVID-19. However, most the methods employed Deep learning algorithms without providing any additional information at the segmentation phase. Hence this paper proposes a new segmentation Mechanism based on the Fuzzy C-Means (FCM) and different features. A new Variant of FCM called as Dual FCM is introduced which forms an objective function based on two different Sub-Objective Functions (SOFs). The first SOF segments the images through gray pixel intestines while the second SOF used features for segmentation. Two different features are derived namely morphological features and gradient features from every CXR image. Finally, the segmented results at individual SOFs are fused to get a final segmented result. Extensive experiments have been carried out over the proposed approach through two publicly available datasets namely Montgomery County **(**MC) Dataset and Shenzhen Dataset. The performance is assessed through two evaluation measures namely Jaccard Index (JI) and Dice Coefficient (DC) and the average obtained is noticed as 92.985% and 95.295% respectively. Further the proposed segmentation mechanism is compared with several past lung image segmentation approaches. The approximate improvement in the JI and DC from past methods is noticed as 4.2210% and 2.3150% respectively.

Keywords: Lung CXR segmentation, FCM, Gradient features, Morphological features, Jaccard index, Dice coefficient.

1. Introduction

Recently, the impact of different types of diseases on the human health is increasing rapidly due to several changes in the environment, lifestyle, climate changes and some other factors. For example, the worldwide death count is approximated as 3.4 million in 2016 due to the Chronic Obstructive Pulmonary Disease (COPD) and it is estimated at approximately 400,000 due to asthma [1, 2]. The main reason behind these deaths is abnormal smoking habits and air pollution. Mainly, these deaths are observed in the countries which are in developing state and have lower income where the air pollution and poverty are totally uncontrollable. According to the statistics of World Health Organization (WHO), the approximate count of pre-mature deaths is 4 million due to the household air polluted diseases like pneumonia and asthma. Pneumonia is found as common lung infecting disease affecting approximately 450 million people per year. It causes due to several reasons like causative virus, bacterial infection and viral infection [3]. On the other hand, the Tuberculosis (TB) which is regarded as a preventable and treatable disease, it remains one of the world's most infectious diseases and taking the lives of approximately 1.6 million annually [4]. In addition to these diseases, the recently evolved COVID-19 caused a serious damage to the lungs and breathing system. According to the WHO standard, the total number of cases confirmed by June 5, 2021 is 172, 242, 495 and the total number of deaths is 3, 709, 397. In the case of India, the spread of COVID-19 is observed as 28,697,879 totally confirmed cases and the deaths are reported as 3, 44, 082 [5]. The first place is occupied by United States of America with the total number of cases

reported is 32,997,875 while the second position is occupied by India with 28,697,879. These are very larger numbers compared to the numbers reported in the first outbreak. Hence, it is necessary to take necessary actions against the air pollution and carbon emissions. In addition, the fast diagnosis of lung diseases also makes the people to survive for longer times.

Recently, the Digital Images based diseases diagnosis has evolved as a new direction of diagnosis which is found as accurate and fast. Here, the digital images like X-ray, Compute Tomography (CT), and Magnetic Resonance Imaging (MRI) are fed as input to computational methods to find the out presence and status of diseases. For instance, the Chest X-Ray (CXR) images can be used to detect and classify different types of lung diseases. Fig. 1 shows some examples of digital images belong to lung diseases. However, the detection and classification of lung diseases from Chest X-ray images is a challenging task. Based on such inspiration, several methods [6-10] have been proposed by several researchers to achieve prominent results in the classification of lung diseases. Moreover, the recent Covid-19 has created so many challenges in the detection of lung diseases in the Computer Aided Diagnosis (CAD) systems. From the past methods [11, 12], the following problems are observed at the detection of lung diseases from Digital Images. (1) Most of the methods employed direct classification methods without finding the Region of Interest (ROI) in the digital image, (2) Less focused on the provision of discrimination between different diseases and (3) Deep learning algorithm are employed which are very complex in nature.

To sort out these problems, this paper proposes a new Digital Lung Image segmentation mechanism which determines the ROI from lung CXR image.

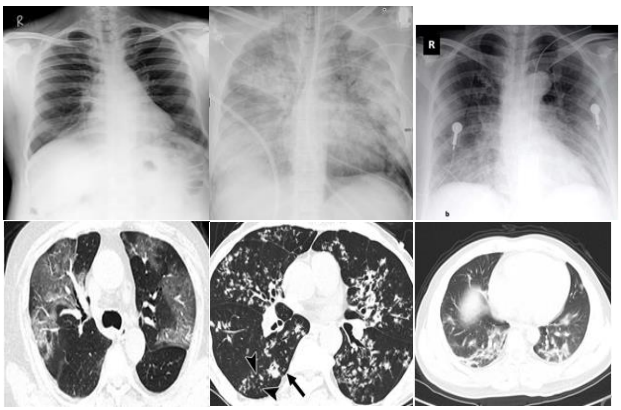

(a) (b) (c)

Figure. 1 1st Row: CXR images and 2nd row: CT images (a) Pneumonia, (b) Tuberculosis, and (c) COVID-19

The major contributions are outlined as follows;

- To improve the segmentation performance, this paper proposes a new FCM called as Dual FCM in which the main objective function is formulated as a combination of two sub-objective functions. One SOF considers the Gray pixel intensities as input and other SOF considers features as input for segmentation.
- To provide a better connectivity between pixels in the segmented regions, a new membership weight metric is introduced and integrated with fuzzy distance function in the main objective function of FCM.
- To explore the more detailed information about the pixels belongingness, it is described through two new feature namely gradient feature and morphological features.

Rest of the paper is structured as follows; the details of related work are discussed in second section. The details of proposed lung image segmentation approach are discussed in third section. Fourth section elaborates the details of experimental investigations and final section concludes the paper.

2. Literature survey

Due to the rise in the automatic diagnosis of lung diseases through digital images and computational methods, several researchers have proposed several methods. For instance, Barhoom and Alaa M. A. [13] focused on the classification of different types of pneumonia (normal, viral and bacterial) through VGG pre-rained model which has totally 16 convolutional layers and a hidden layer. In addition, they introduced a dropout layer which helps in regularizing the model by preventing the model from over fitting. Totally they simulated their model on nine thousand CXR images. However, they experienced more misclassifications between viral and bacterial due to insufficient discrimination.

Next, A. Sadiya *et al.* [14] applied three machine learning algorithms for the classification of Pneumonia from TB. The three algorithms are namely Gaussian Naïve Bayes, Random Forest and Decision tree. Processing the raw images to classifiers introduced more ambiguity followed more false positive rate. R. Mogaveera *et al.* [15] aimed at the Multi-class classification from CXR images through ConvNets. Each CXR image is classified into three classes Namely Normal, Pneumonia and Tuberculosis. As a preprocessing, they resized the CXR image into a uniform size of 256×256 and then employed three data augmentation methods to rotate, scale and contrast enhancement. Four convolution layers, three pooling layer and four fully connected layers are designed in their ConvNet

model. However, the image translation introduces additional features which don't have a proper significance in the disease diagnosis.

M. Abubakar *et al.* [16] employed Inception and VGG-16 based deep learning architectures to classify the CXR images into three classes namely Normal, Pneumonia and Tuberculosis. As a part of pre-processing, they resized each CXR image into a uniform size of 90×90 followed by gray scale conversion. They obtained an accuracy of only 92.97%. Without the extraction of Region of Interest, the classification of lung CXR images experiences more Misclassifications. O. Stephen *et al.* [17] proposed a new Convolutional Neural Network (CNN) model for the classification of pneumonia and non-pneumonia in CXR images. The CNN model consists of 4 convolution layers, for pooling layers, two fully connected layers, one dropout layer and one flatten layer. At pre-processing, they performed image augmentation through rotating, scaling, shifting, shearing and flipping. However, all these methods applied deep learning algorithms over the CXR images without any additional processing and hence resulted in poor classification accuracy.

Some authors applied deep learning algorithms for the segmentation of lung region from CXR and CT images. A. S. Brahim *et al.* [18] segmented the lung CT image through U-net architecture which is found as one of the mostly employed architecture in deep learning algorithm for the segmentation of images. U-Net architecture recovers the required information through a symmetric expanding path and extracts high level information through contracting path. However, U-Net needs more parameters tuning which results in more computational complexity. A. Saood and I. Hatem [19] proposed to employ two deep learning networks namely U-Net and SegNet for the classification of Lung CT image. U-Net is characterized as a toll for segmentation while the SegNet is regarded as a network for segmentation. Both models are considered as Binary Segmentors which can discriminate between healthy and infected tissue. In addition, they also considered as multi-class Segmentors which can classify the type of infection in the lungs. But, the U-Net and SegNet models has major disadvantage of over-fitting due to the process lager parameters tuning.

To solve the problems with U-Net, W. Liu *et al.* [20] proposed an improved version of U-net for the segmentation of lung CXR images. Their U-net model used the pre-training Efficientnet-b4 for encoding and the combination of LeakyReLU and Residual Block for decoding. Compared to the traditional U-net, the improved U-net gained an improvement of 6% Jaccard index and 2.5% dice coefficient. Another improved version of U-Net is proposed by T. W. Chiu *et al.* [21] called as 2D U-Net for the segmentation of lung nodule from CT images. They mainly concentrated on the removal of data imbalance problem in the deep learning models at classification of background and foreground where lung nodule is considered as foreground and remaining regions' is considered as background. However, they simulated their model on only few CXR images and hence the improved U-Net experienced over-fitting due to the skip connections and additional layers in the expanded path.

However, the U-net and its variants perform poorly in the segmentation of smaller structures and they cannot segment the boundaries of lungs accurately. Hence, Further, X. Xu *et al.* [22] proposed a new fusion network based on the interaction between multiple features extracted through two new models namely U-Net and KiU-Net. KiU-Net and U-Net extracts the detailed and high level features from the lung images respectively. Then they employed a cross-residual fusion module to get the complimentary information from the two networks. At last, a multi-interaction module is introduced to ensure a hassle-free interaction between multiple features like branching features, contextual features and fused features. Another variant of U-net called as Residual U-Net is proposed by E. Mique and A Malicdem [23] which integrates the residual blocks into the deep U-net architecture. However, the involvement of Residual blocks in U-Net increased the computational complexity at Lung image segmentation.

A. Jaszcz *et al.* [24] proposed to use the Red Fox Heuristic Optimization Algorithm (RFOA) to segment the lung CXR image. A new fitness function is proposed and applied RFOA for the optimization of threshold in such a way the two regions are segmented in an efficient manner; they are lung region and non-lung region. A publicly available dataset is used for the experimental validation. RFOA considered only pixel intensities a as input values and hence, it explored poor performance at the segmentation of CXR images.

Summary of Problem: the major problem identified with the existing method is their larger misclassification of lung pixels. Due to the direct accomplishment of segmentation algorithms over the CXR image, they experienced more ambiguity at the clustering of lung pixels and background pixels into different clusters. In addition, the segmentation is a simple task which at least required the complex deep learning algorithms.

3. Proposed segmentation model

3.1 Overview

This section explores the complete details of proposed lung image segmentation model. Unlike the existing methods which considers direct image pixel intestines for segmentation through either machine learning or deep learning algorithms, this model considers gradient features in addition to pixel intensities for segmentation. The major novelty of the proposed model is Dual FCM which involves two individual FCMs; one is based of pixel intestines and another is based on gradient features. Fig. 2 shows an example of proposed segmentation model for lung images. According to the block diagram, the entire methodology is accomplished din two phases; they are preprocessing and unsupervised segmentation. The main aim of preprocessing is to enhance the quality of lung image such that the all regions will appear clearly. For this purpose, we applied the most popular Contrast Limited Adaptive Histogram Equalization (CLAHE) which adjusts the contrast levels of pixels based on the dynamic thresholds. Fig. 3 shows the results of CLAHE on different CXR and CT lung images. Then the quality enhanced image s fed as input to dual FCM for the segmentation of lung region. The details of segmentation are explored in the following subsections.

3.2 Segmentation

The overall segmentation is carried out in two phases; they are pixel based segmentation and feature based segmentation. At both phases, we applied FCM as segmentation methodology. Unlike the conventional methods which applies segmentation methods directly over the lung images, this method applied in two different ways; they are (1) Over Gradient features and (2) Over pixels. The details of gradient features extraction and Dual FCM are explored in the following subsections.

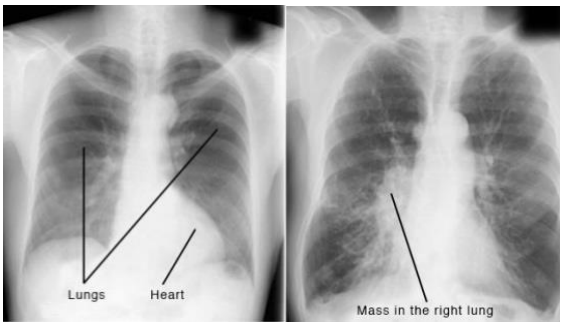

(a) (b)

Figure. 2: (a) Normal Lung CXR and (b) Diseases Infected lung CXR image

3.2.1 Segmentation

***A. Gradient Features*:** Gradient features are the most prominent features which gained huge popularity in several image processing applications. The gradient of an image gives information about the directional change of the color or intensity in an image. For instance, the canny edge operator uses image gradient for the detection of edges in images. The gradients help in providing sufficient information about the presence of different regions in images.

In the case of normal lung CXR or CT images, the lung portion is totally different from other parts of images. On the other hand, in the case of the disease infected lung images, the lung portion comprises of different abstractive regions like pneumonia, additional mass (see Fig. 3) etc. In such cases, the accomplishment of gradients over lung images differentiates the regions effectively. Hence, this paper considers extracting the gradient features from lung image to do the segmentation. The gradient is simply defined as Directional derivative of scalar field. Gradient gives information about the image. The gradients are calculated in two directions, they are vertical and horizontal directions. Based on these two gradients, the final gradient magnitude and the corresponding direction are measured. Considering this fact, here we represent each pixel with four gradient features they are G_x, G_y, G_M and G_θ . They are calculated as follows.

$$G_x(x,y) = |C(x+1,y) - C(x-1,y)| \quad (1)$$

$$G_y(x,y) = |C(x,y+1) - C(x,y-1)| \quad (2)$$

$$G_M(x,y) = \sqrt{\left(G_x(x,y)\right)^2 + \left(G_y(x,y)\right)^2} \quad (3)$$

$$G_\theta(x,y) = \tan^{-1}\left(\frac{G_y(x,y)}{G_x(x,y)}\right) \quad (4)$$

Where $G_x(x,y)$ is the gradient of pixel (x,y) along X-direction and $G_y(x,y)$ is the gradient of pixel (x,y) along Y-direction, $G_M(x,y)$ is the magnitude of a gradient and $G_\theta(x,y)$ is the direction of a gradient $G_M(x,y)$. We explore the difference between successive pixels and $G_\theta(x,y)$ and express the direction of movement of the corresponding pixel. Fig. 4 shows some examples of original CT images and their corresponding gradient images. Similarly, Fig. 5 shows some examples of original CXR images and their corresponding gradient images.

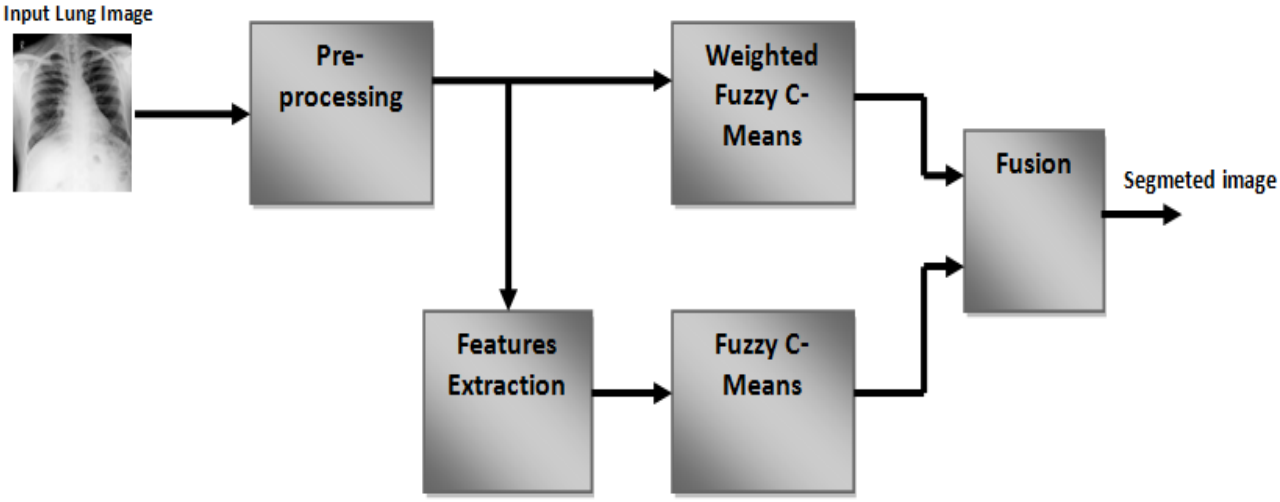

Figure. 3 Block diagram of proposed segmentation model

***B. Morphological features*:** Mathematical Morphology (MM) is one of the prominent strategies for image segmentation. MM is employed through two operators; they are erosion and dilation. Erosion operation separates the linked objects by diminishing them and it widens the holes. On the other hand, the dilation operation connects the objects by filling the holes. The erosion operation followed by the dilation operation is called as morphological opening and dilation followed by erosion is called as morphological closing. For any mathematical

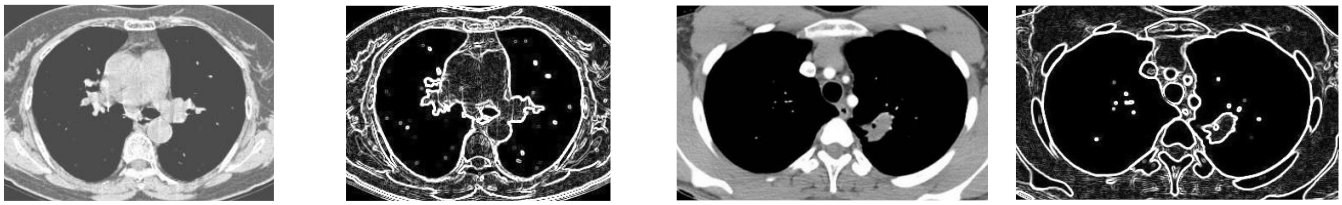

(a) (b) (c) (d)

Figure. 4: (a) Input CT lung image, (b) gradient CT image, (c) Input CT lung image, and (d) gradient CT image

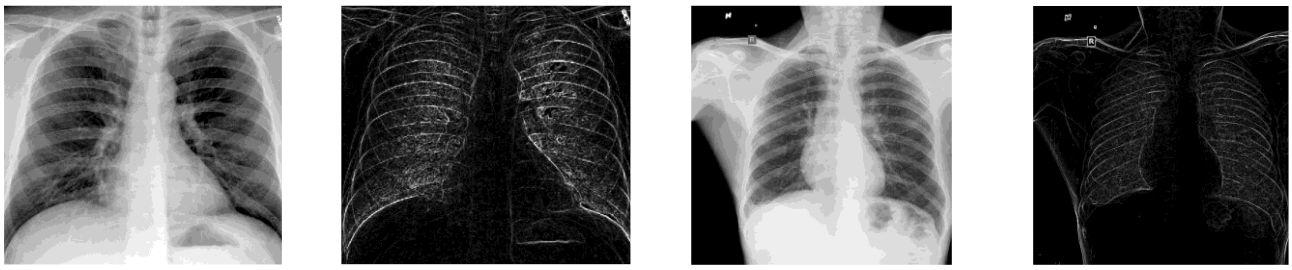

(a) (b) (c) (d)

Figure. 5: (a) Input CXR lung image, (b) gradient CXR image, (c) Input XR lung image, and (d) gradient CXR image

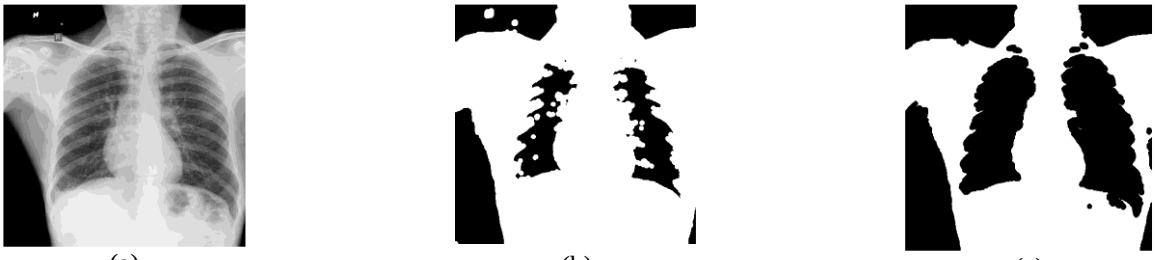

(a) (b) (c)

Figure. 6 Morphology results: (a) Input CT and CXR image, (b) Morphologically Eroded Image, and (c) Morphologically Dilated Image

morphology operation, one structuring element is required and it varies based on the structure and shape of the object. The Structuring element is placed in such a way that the pixel is located at centre. We used top-hat and bottom-hat transforms under mathematical morphology features. These two methods help in the provision of perfect differentiation between lung pixels and background pixels. Top –hat transform acts like a HPF and it extracts brighter areas and bottom hat transform extracts the darker regions. Mathematically these two can be represented as

$$T_H(C) = C - (C°SE) \tag{5}$$

$$B_H(C) = (C \cdot SE) - C \tag{6}$$

Where ° denotes the opening operation and · denotes closing operation. The dimension of structuring element maintained is one pixel in width and 15 pixels in length. Fig. 6 shows the results of morphology.

3.2.2 Dual FCM

Dual FCM is accomplished in two stages; in the first stage, FCM considers gray pixel intensities as input and performs segmentation whereas the 2nd stage considers features as input and performs segmentation. In summary, the overall objective function of formulated as function of two Sub-Objective Functions (SOFs). The first SOF considers the gray pixel intensities from the raw CXR image. In the cases of 2nd SOF, it is again realized as a combination of two functions, the first function checks the pixels connectivity with neighbor pixels while the 2nd function considers features extracted from the image. Based on these two SOFs, the final objective function is formulated as the minimum of SOF1 and SOF2. According to the theory, the objective function of Dual FCM is formulated as

$$F = \min(f_1 + f_2) \tag{7}$$

Where f_1 and f_2 are the two SOFs and F is the minimum of two SOFs. According to the standard theory of FCM, i.e., clustering based on the minimization of distance between clusters and pixels, the f_1 is written as

$$f_1 = \sum_{i=1}^{M} \sum_{j=1}^{C} u_{ij}^m \left\| p_i - c_j \right\|^2 \tag{8}$$

Where u_{ij} is called as membership degree of the pixel (p_i) with cluster center (c_j), m is the parameter of fuzziness and its nominal value is fixed to 2. In FCM, the clustering is done after the computation of Euclidean distances between each pixel with each cluster center. A pixel *i* with larger membership with a cluster center *j* gets clustered into the cluster where the j is a cluster center. So, the membership decides the pixels cluster and it is mathematically computed as

$$u_{ij} = 1 \Big/ \left(\sum_{k=1}^{C} \left(\frac{d_{ij}}{d_{ik}} \right)^{\left(\frac{2}{m-1} \right)} \right) \tag{9}$$

Next, the mathematical expression for the computation of cluster center is expressed as

$$V_j = \left(\sum_{i=1}^{M} (u_{ij}^m) x_i \right) \Big/ \left(\sum_{i=1}^{M} (u_{ij}^m) \right), \quad \forall\, j = 1,2,3, \ldots, C \tag{10}$$

Where M denotes the total pixels count and $\left\| p_i - c_j \right\|$ denotes the Euclidean distance between pixel (p_i) and cluster center (c_j). Eq. (8) iterates for multiple times until the convergence happens, i.e., all the pixels are successfully clustered into at least one cluster. At each iteration, the cluster center of each cluster is updated based on the membership values computed in Eq. (9).

However, the FCM experiences higher computational complexity in terms of more number of iterations when the fuzziness parameter is low. Further, the computation of Euclidean distance based membership computation can unequally weight the underlying factors. In addition, FCM shows poor segmentation results in the presence of noise or outliers in the data. Hence, we modified the FCM by introducing a new parameter called as Membership Weight (w_{ik}) which computes the correlation between center pixel and its neighbor pixels. The main reason behind w_{ik} is the high correlation between adjacent pixels. Towards such weight computation, this approach slides a window over the image by keeping each pixel at the center. For example, if the size of window is assumed as 3×3, then the total number of neighbor pixels surrounded the centre pixel becomes 8. Then the weight of center pixel (w_i) is computed as an average of membership weights of surrounding pixels. Mathematically, it is expressed as

$$w_i = \sum_{k=1}^{K-} w_{ik} \; \forall\, k \in 1,2,3, \ldots, K \tag{11}$$

Where w_{ik} is computed as the membership weight of

k_{th} pixel with center pixel i. mathematically, it is expressed as

$$w_{ik} = \begin{cases} p_i - p_k, & if\ p_i - p_k > \mu_i \\ 0, & otherwise \end{cases} \quad (12)$$

Where μ_i is the mean deviation between center pixel p_i and surrounding pixels. It is calculated as an average of deviation between center pixel and surrounding pixel. The mathematical expression for μ_i is given as

$$\mu_i = \frac{1}{size(\omega)} \sum_{k=1}^{K} (p_i - p_k) \forall\ k \in 1,2,3, \ldots., K \quad (13)$$

Where K denotes the total pixel count surrounding the center pixel and *K*- denotes the pixel satisfied the condition in Eq.(12). For a 3×3 sized window, K becomes 8 and hence the K- is less than 8. Similarly for a 5×5 sized window, K becomes 24 and hence the K- is less than 24. In this way, the membership weight is calculated for each pixel and it is integrated with the fitness function. According to this theory, the modified fuzzy distance function is written as $\|p_i - c_j\|^2 (w_i)$.

Next, the 2nd SOF considers the feature vector as input to perform the segmentation. Here, the feature vector is obtained based on the concatenation of gradient features and morphological features. So, every pixel in the lung image is replaced with a feature vector and then fed to FCM. Consider a pixel at the position (x, y) is represented with $p(x, y)$, it is replaced with the newly derived feature vector $GM_f(x, y)$ which is a concatenated form of two features namely gradient feature $G_f(x, y)$ and morphological feature $M_f(x, y)$. Then the objective function of FCM is expressed in terms of feature vectors as

$$f_2 = \sum_{i=1}^{M} \sum_{j=1}^{C} u_{ij}^m \left\| GM_f^i - c_j \right\|^2 \quad (14)$$

Where GM_f^i represents the i_{th} feature and c_j is the j_{th} cluster center. Similar to the FCM, the feature based FCM also finds out the membership and updates the cluster center at every iteration. The updating is done until the convergence occurs where each pixel gets clustered into at least one cluster.

4. Experimental analysis

This section explores the particulars about the experimental investigations on the proposed approach. To validate the proposed lung segmentation mechanism, we consider the CXR images from two standard publicly available datasets they are MC Dataset [25] and Shenzhen dataset [26]. The experiments are conducted on a Personal computer with 1TB hard disk and 8 GB RAM and MATLAB tool is used for simulation coding. In this section, we initially explore the details of datasets, then the performance metrics and finally the results derived from the experiments.

4.1 Datasets

MC Dataset: This dataset consists of totally 138 CXR images among which 58 images are belong to tuberculosis patients and 80 images are belongs to normal patients. MC Dataset images are created by the US national Library of Medicine and named after Montgomery County (MC). Each image is in the *.png* format and have the resolution of 4020×4892. Each chest X-off image belongs to a masked image of the lung. This dataset consists of various lung shapes and tissues due to several disorders like corpuscular lesions and pleural effusion. Fig. 7 shows some examples of lung CXR images of MC Dataset and their corresponding segmented results.

Shenzhen Dataset: This is one more standard and poplar CXR image dataset which consist of totally 662 CXR images among which 326 are belongs to normal patients and 336 are belongs to the patients with different abnormalities. The images available in this dataset are collected from a Hospital in Shenzhen, Guangdong Province, China. However, this dataset has only 566 lung masks. Each image is in the *.png* format and have the resolution of 2919×3000. Fig. 8 shows some examples of lung CXR images of Shenzhen dataset.

4.2 Performance metrics

Further, for subjective analysis, several performance metrics are considered. Firstly, some reference measures like False Positive (FP), False Negative (FN), True Positive (TP) and True Negative (TN) are evaluated based on the obtained segmentation results. The formal definitions of these measures are given below;

(i) TP: Total number of Lung pixels those classified as Lung pixels.
(ii) TN: Total number of non- Lung pixels those classified as non- Lung pixels.
(iii) FP: Total number of Non- Lung Pixels those classified as Lung Pixels.
(iv) FN: Total number of Lung Pixels classified as Non- Lung Pixels

Based on these secondary metrics we compute two metrics namely Jaccard Similarity index and Dice

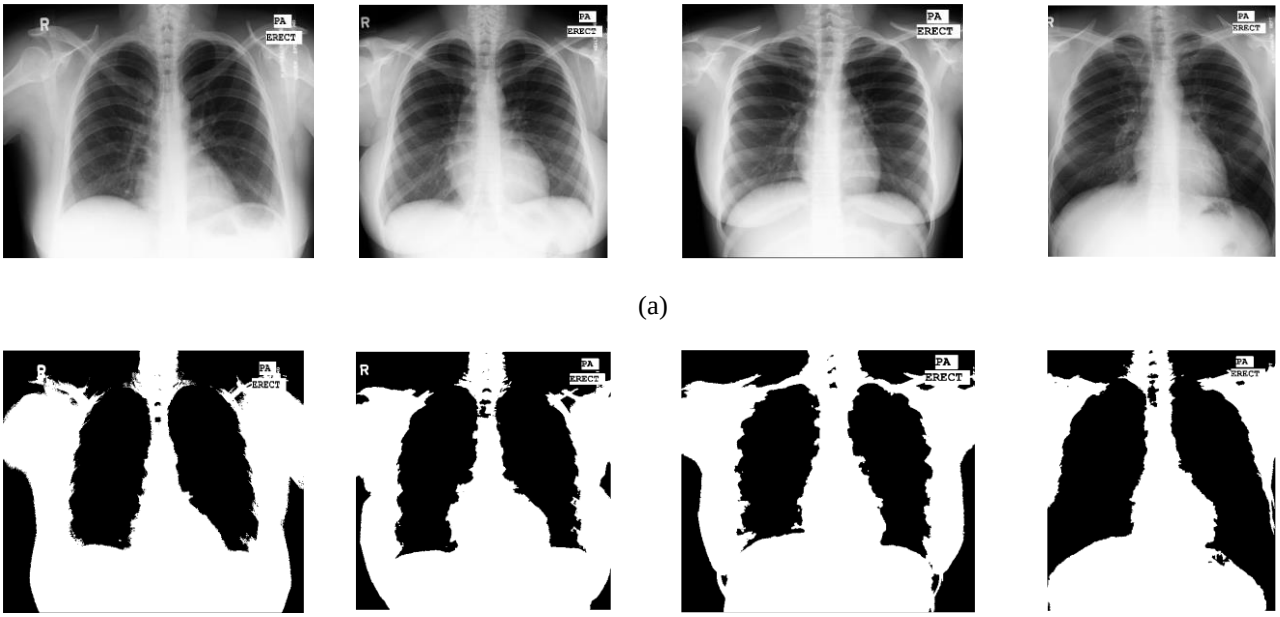

Figure. 7: (a) Samples CXR images of MC Dataset and (b) Segmented resultant images

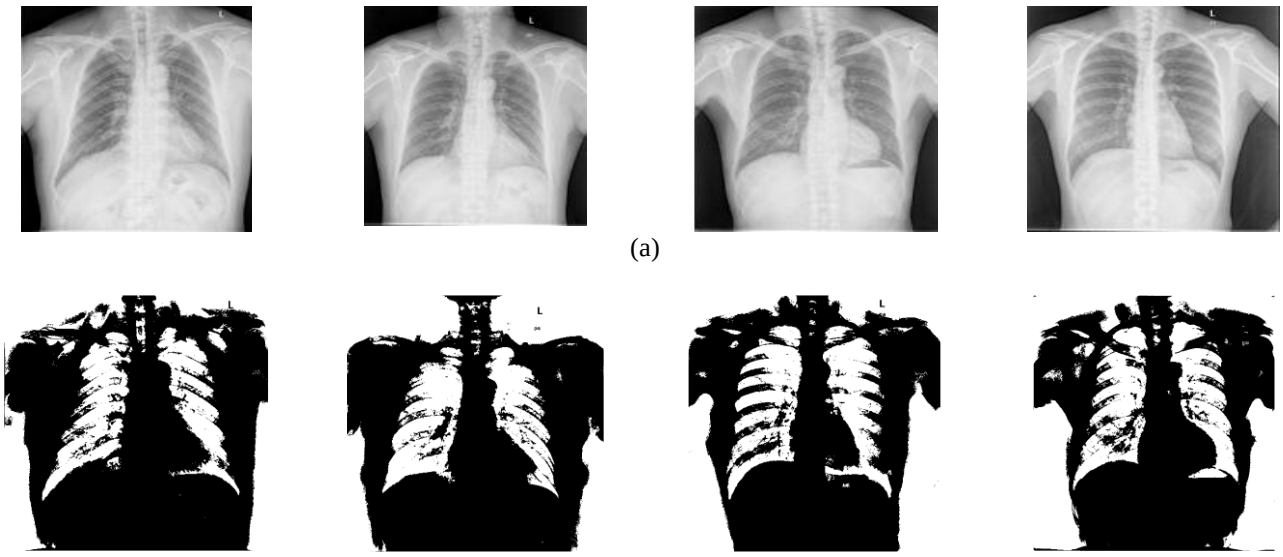

Figure. 8: (a) Samples CXR images of Shenzhen Dataset and (b) Segmented resultant images

Similarity Index. Consider two binary images A and B, they are calculated as follows;

$$J(A,B) = \frac{|A \cap B|}{|A \cup B|} = \frac{TP}{TP+FP+FN} \quad (15)$$

$$D(A,B) = \frac{2*|A \cap B|}{|A|+|B|} = \frac{2TP}{2TP+FP+FN} \quad (16)$$

In this work, A is considered as the ground truth lung mask provided by the database creators and B as the segmented lung portion image and they are processed for assessment in their binary form only. The confusion matrices are formulated based on the classified pixels into either lung pixel or non-lung pixel.

4.3 Results

Table 1 shows the performance analysis of proposed approach on different CXR images of MC Dataset. We have tested the proposed segmentation approach on totally 100 CXR images but due to space limitation we have kept only the results of first 20 images. From the results, it was observed that the proposed segmentation mechanism has gained better performance because the values of Jaccard Index and Dice Coefficient are all almost above 0.90.

Table 1. performance analysis of proposed approach on MC Dataset

Image Sample	Jaccard Index	Dice Coefficient	Image Sample	Jaccard Index	Dice Coefficient
MCUCXR_0001_0	0.9562	0.9845	MCUCXR_00016_0	0.9333	0.9967
MCUCXR_0002_0	0.9365	0.9635	MCUCXR_00017_0	0.8964	0.9269
MCUCXR_0003_0	0.9045	0.9567	MCUCXR_00019_0	0.8789	0.9138
MCUCXR_0004_0	0.9145	0.9478	MCUCXR_00020_0	0.8647	0.9147
MCUCXR_0005_0	0.8865	0.9245	MCUCXR_00021_0	0.9045	0.9365
MCUCXR_0006_0	0.8962	0.9178	MCUCXR_00022_0	0.8845	0.9378
MCUCXR_0008_0	0.9052	0.9368	MCUCXR_00023_0	0.9230	0.9638
MCUCXR_00011_0	0.9632	0.9968	MCUCXR_00024_0	0.8649	0.9167
MCUCXR_00013_0	0.9145	0.9578	MCUCXR_00026_0	0.8875	0.9239
MCUCXR_00015_0	0.9235	0.9645	MCUCXR_00027_0	0.9041	0.9544

Table 2. performance analysis of proposed approach on Shenzhen Dataset

Image Sample	Jaccard Index	Dice Coefficient	Image Sample	Jaccard Index	Dice Coefficient
CHNCXR_0001_0	0.9132	0.9452	CHNCXR_00011_0	0.9063	0.9478
CHNCXR_0002_0	0.9012	0.9333	CHNCXR_00012_0	0.8678	0.9063
CHNCXR_0003_0	0.8795	0.9045	CHNCXR_00013_0	0.8456	0.8895
CHNCXR_0004_0	0.8891	0.9147	CHNCXR_00014_0	0.8369	0.8723
CHNCXR_0005_0	0.8562	0.8865	CHNCXR_00015_0	0.8745	0.9078
CHNCXR_0006_0	0.9643	0.9965	CHNCXR_00016_0	0.8555	0.8867
CHNCXR_0007_0	0.8795	0.9045	CHNCXR_00017_0	0.8967	0.9327
CHNCXR_0008_0	0.9352	0.9653	CHNCXR_00018_0	0.8945	0.9247
CHNCXR_0009_0	0.8836	0.9145	CHNCXR_00019_0	0.8365	0.8636
CHNCXR_00010_0	0.8945	0.9278	CHNCXR_00020_0	0.8765	0.9169

Table 3. Comparison between proposed and existing methods

Reference	Dataset Used	Jaccard Index (JI)	Dice Coefficient (DC)
M. F. Rahman et al. [34]	MC	89.1300	94.2500
A. Singh et al. [32]	MC & Shenzhen	90.0000	95.000
Chen et al. [30]	MC	83.1000	88.6400
W. Nimalsiri et al. [31]	MC	91.9700	-
F. Cao and H. Zhao [27]	Shenzhen	91.2600	95.4500
Bosdelekidis et al. [33]	MC	86.2000	92.3200
Munawar et al. [29]	MC	91.7000	93.8300
	Shenzhen	90.6000	93.7700
Kim et al. [28]	MC	92.4000	94.2200
	Shenzhen	90.2000	92.4300
Proposed	MC	**94.5200**	**95.9600**
	Shenzhen	**91.4580**	**94.6380**

Such values indicate that the proposed approach has segmented approximately 90% of lung pixels as same. For MC Dataset, the average Jaccard Index is observed as 0.9301 and the average dice coefficient is observed as 0.9551. Similarly, the performance analysis of proposed approach on Shenzhen Dataset is shown in Table 2. In this case, we have tested out segmentation mechanism on totally 500CXR images and kept in the results of twenty images. For Shenzhen Dataset, the average Jaccard Index is

observed as 0.8996 and the average dice coefficient is observed as 0.9293. Since the images of Shenzhen Dataset are composes of muscles and bones in the chest x-ray, the two-class segmentation mechanism misclassified some of the lung pixels as other region's pixels. Hence the proposed approach experienced less segmentation performance in Shenzhen dataset when compared with the MC Dataset.

To assess the impact of features on the segmentation of lung images, we conducted a case study be feeding individual features and gray pixel intensities individually. The results about Jaccard Index are shown in Fig. 9 and Dice Coefficient is shown in Fig. 10. From the analysis, we determined that the proposed Dual FCM outperformed the individual FCMs where either features or gray pixel intensities are considered as points. Here, FCM-features denote that the FCM considered features as input and FCM-intensities denotes that the FCM considered raw pixel intensities as input. Among these two methods, the features based FCM had shown better segmentation performance, especially for Shenzhen Dataset. In the case of MC Dataset, the both methods had shown approximately equal performance, as the FCM-features gained an average Jaccard Index of 0.8920 while FCM-Intensities gained an average Jaccard Index of 0.8960. But, for the Shenzhen Dataset, the average Jaccard Index of FCM-Features is observed as 0.8550 whereas the FCM-intensities gained only 0.8410. Similarly, the average Dice Coefficient of FCM-Features is observed as 0.8956 whereas the FCM-intensities gained only 0.8742. Based on these observations, it can be stated that the features can provide more knowledge about the characteristics of lung portion than the just pixel intensities.

Table 3 shows the Comparison between proposed and existing methods at different datasets through Jaccard Index and Dice Coefficient. F. Cao and H. Zhao [27] introduced a variational auto-encoder (VAE) for lung CXR image segmentation in every layer of encoder and decoder. VAE can extract the high level semantic features which explores the symmetrical relationship between pixels. At the same time, they introduced three attention mechanisms to get the target area from image. However, the VAE adds an additional computational burden on the segmentation system.

Kim et al. [28] applied a self-attentive module in the U-net architecture to segment the lung portion from CXR images. For MC Dataset, they gained an average JI of 92.4000 and average DC of 94.2200 and for Shenzhen dataset they gained an average JI and DC are of 90.2000 and 92.4300 respectively.

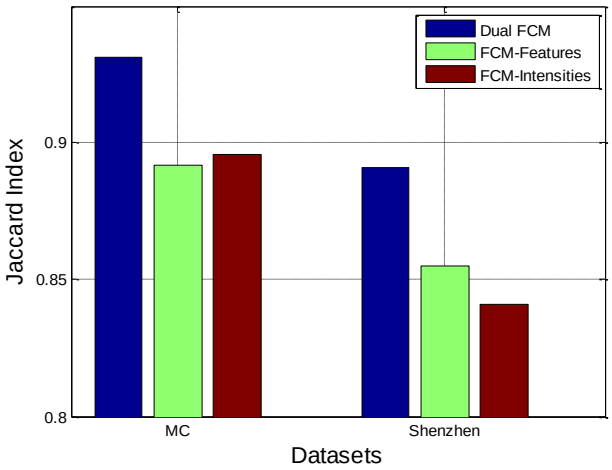

Figure. 9 Jaccard Index analysis at different FCMs

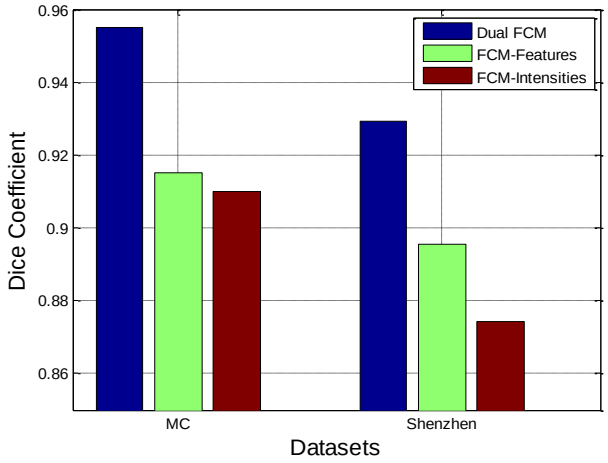

Figure. 10 Dice Coefficient analysis at different FCMs

Next, Munawar et al. [29] applied the Generative Adversarial Networks (GANs) for the segmentation of lung CXR images. They used the skip connections of U-net which helps in the preservation of morphology and also reduces the risk of vanishing gradient. They used both MC and Shenzhen datasets and gained an appreciable performance at the segmentation. Next, Chen et al. [30] initially enhanced the contrast levels of CXR image and then processed it for the adaptive image binarization to segment background from foreground. Finally, they employed CNN based architecture to train the binarized images for segmentation. For experimental validation, they used MC Dataset and gained 83.1000 JI and 88.6400 DC. Training the binarized imaged for lung segmentation can show excellent performance on only known images but have very limited performance on unknown images and noisy images.

W. Nimalsiri et al. [31] proposed a U-net model with spatial attention (SA-UNet) for the segmentation of lung CXR images. Based on the inspiration of MC Dataset, they have created a new dataset and applied the SA-UNet on the both datasets.

However, due to the presence of skip connection in UNet, they gained only 91.9700 JI on the MC Dataset.

A. Singh et al. [32] used a deep learning model for automatic segmentation of CXR images. Their model comprised of 20 fully convolutional layers which can simplify the images to precisely section the lung lobes from CXR image. Two datasets namely MC and Shenzhen are used for experimental analysis and gained an average JI and DC of 90.0000 and 95.0000 respectively.

Bosdelekidis et al. [33] considered the bone structure as reference for lung segmentation and proposed a two-step approach through a sparse representation of the rib cage guided to different support points on the border of lung. They gained an average DC of 92.3200 and average JI of 86.2000 on MC Dataset.

M. F. Rahman et al. [34] introduced a two-stage framework based on the –Net architecture to perform an automatic lung CXR image segmentation. In the 1st stage, they extract CXR patches and train the modified U-Net model to get the initial segmentation of lung field. Next, the 2nd stage is focused on post-processing where they apply image processing methods to get the clear and final segmented result. They simulated totally on 138 CXR images from MC Dataset and gained an average DC of 94.2500 and JI of 89.1300.

Compared with the above methods, the proposed method is very simple as it accomplished the FCM algorithm which has very much less computational complexity than the deep learning algorithms like U-Net and its updated versions. Instead of applying the deep learning algorithm directly for segmentation, a pre-processing before segmentation improves the performance. In the proposed model, the gradient and morphological features had shown their contribution in perfectly discriminating the lung pixels and background pixel in CXR image. Hence the proposed model gained better performance than all the existing methods.

5. Conclusion

This paper mainly aimed at the segmentation of lung portion from CXR images and towards such prospect a new unsupervised learning assisted segmentation method is proposed. A new version of FCM called as Dual FCM is introduced here which considers not only the pixel intensities and also the features as the input data. Two set of features namely morphological and gradient features are extracted from CXR image and fed as a composite vector to FCM for segmentation. The former features explore the discrimination between regions and later features explore the connectivity between pixels in the same region. Extensive simulations on MC and Shenzhen datasets prove the efficacy in terms of Jaccard Index and Dice Coefficient. At comparison, the proposed segmentation model had shown excellent performance than the existing methods at both datasets. The average improvement in the DC is observed as 2.3150% while for JI, it is observed as 4.2210% from the existing approaches.

Conflicts of Interest

The authors declare no conflict of interests.

Author Contributions

Conceptualization, Design, Development and implementation of proposed method by Duvva Naresh and Validation and proofread by M. Kezia Joseph.

References

[1] S. Bharati, P. Podder, R. Mondal, A. Mahmood, M. Raihan-Al-Masud, "Comparative performance analysis of different classification algorithm for the purpose of prediction of lung cancer", *Advances in intelligent systems and computing*, Vol. 941, pp. 447-57, 2020.

[2] N. Coudray, P. S. Ocampo, T. Sakellaropoulos, "Classification and mutation prediction from non–small cell lung cancer histopathology images using deep learning", *Nat. Med.*, Vol. 24, pp.1559-67, 2018.

[3] M. R. H. Mondal, S. Bharati, P. Podder, "Data analytics for novel coronavirus disease," *Iinformatics in medicine unlocked*, Vol. 20, pp. 100374-100386, 2020.

[4] K F Larsen, C D Wells, "Reaching the targets for tuberculosis control: the impact of HIV", *Bull World health Organ*, Vol. 85, No. 5, pp.377-381, 2007.

[5] WHO Coronavirus (COVID-19) dashboard;, available at https://covid19.who.int/.

[6] W. Yang, A. Sirajuddin, X. Zhang, G. Liu, Z. Teng, S. Zhao, M. Lu, "The role of imaging in 2019 novel coronavirus pneumonia (COVID-19)", *Eur Radiol.* Vol. 15, pp.1-9, 2020.

[7] S. Kundu, H. Elhalawani, J. W. Gichoya, C. E. Kahn, "How might AI and chest imaging help unravel COVID-19's mysteries?" *Radiol: Artif Intell.* Vol. 6, No. 2, pp.e200053, 2020.

[8] M. Y. Ng, "Imaging profile of the COVID-19 infection: radiologic findings and literature review", *Radiol. Cardiothorac. Imaging.*, Vol. 2, No. 1, pp. e200034, 2020.

[9] S. T. H. Kieu, A. Bade, M. H. A. Hijazi, H. Kolivand, "A Survey of Deep Learning for Lung Disease Detection on Medical Images: State-of-the-Art, Taxonomy, Issues and Future Directions", *J. Imaging,* Vol. 6, No. 12, pp.131-145, 2020.

[10] A. Dawadikar, A. Srivastava, N. Shelar, G. Gaikwad and A. Pawar, "Survey of Techniques for Pulmonary Disease Classification using Deep Learning," In: *Proc. of IEEE 7th International conference for Convergence in Technology (I2CT),* Mumbai, India, pp. 1-5, 2022.

[11] M. R. V, S. J, S. Koshy and N. G M, "A Survey on Lung Disease Diagnosis using Machine Learning Techniques," In: *Proc. of 2nd International Conference on Advance Computing and Innovative Technologies in Engineering (ICACITE),* Greater Noida, India, pp. 01-04, 2022.

[12] S. Taha Ahmed, S., & S. M. Kadhem, "Using Machine Learning via Deep Learning Algorithms to Diagnose the Lung Disease Based on Chest Imaging: A Survey", *International Journal of Interactive Mobile Technologies,* Vol. 15, No. 16, pp. 95-112, 2021.

[13] Barhoom, and M. A. Alaa, "Pneumonia diagnosis using deep learning", *PhD dissertation*. Al-Azhar University-Gaza, 2019.

[14] A. Sadiya, A. V Illur, A. Nanda, E. Rao, K. P. Vidyashree, M. Ahmed, "Differential Diagnosis of Tuberculosis and Pneumonia using Machine Learning", *International Journal of Innovative Technology and Exploring Engineering,* Vol. 8, No. 6S4, pp.245-250, 2019.

[15] R. Mogaveera, R.Maur, Z. Qureshi and Y. Mane, "Multi-class Chest X-ray classification of Pneumonia, Tuberculosis and Normal X-ray images using ConvNets", In: *Proc. of International Conference on Automation, Computing and Communication,* Navi Mumbai, India, pp.1-6, 2022.

[16] M. Abubakar, I. Shah, W. Ali, F. bashir, "Classification of Pneumonia and Tuberculosis from Chest X-rays", *arXiv:2103.14562,* 2021.

[17] O. Stephen, M. Sain, U. Joseph Maduh, and D. Jeong, "An Efficient Deep Learning Approach to Pneumonia Classification in Healthcare", *Hindawi Journal of Healthcare Engineering,* Vol. 2019, Article ID 4180949, pp.1-7, 2019.

[18] A. S. Brahim, A. E. L. Hassani, A. Majda, "Lung CT Image Segmentation Using Deep Neural Networks", In: *Proc. of International Conf. On Intelligent Computing in Data Sciences,* Kerala, Iraq, pp.109-113, 2018.

[19] A. Saood and I. Hatem, "COVID-19 lung CT image segmentation using deep learning methods: U-Net versus SegNet", *BMC Med Imaging,* Vol. 21, No. 19, pp.1-10, 2021.

[20] W. Liu, J. Luo, Y. Yang, W. Wang, J. Deng & L. Yu, "Automatic lung segmentation in chest X-ray images using improved U-Net", *Scientific Reports,* Vol. 12, No.8649, pp.1-10, 2022.

[21] T. W. Chiu, Y. L. Tsai & S. F. Su, "Automatic detect lung node with deep learning in segmentation and imbalance data labeling", *Scientific Reports,* Vol. 11, No. 11174, pp.1-10, 2021.

[22] X. Xu, M. Lei, D. Liu, M. Wang, L. Lu, "Lung segmentation in chest X-ray image using multi-interaction feature fusion network", *IET Image Process.,* Vol. 17, No. 14, pp.4129-4141, 2023.

[23] E. Mique and A Malicdem, "Deep Residual U-Net based lung image segmentation for lung disease detection", In: *Proc. of International Conference on Information Technology and Digital Applications,* Yogyakarta, Indonesia, Vol. 803, pp.1-9, 2019.

[24] A. Jaszcz, D. Połap, and R. Damaˇseviˇcius, "Lung X-Ray Image Segmentation Using Heuristic Red Fox Optimization Algorithm", *Hindawi Scientific Programming,* Vol. 2022, Article ID 4494139, pp.1-8, 2022.

[25] S. Candemir, S. Jaeger, J. Musco, Z. Xue, A. Karargyris, S. K. Antani, G. R. Thoma, K. Palaniappan, "Lung segmentation in chest radiographs using anatomical atlases with non-rigid registration", *IEEE Trans Med Imaging.,* Vol. 33, No. 2, pp.577-590, 2014.

[26] S. Jaeger, A. Karargyris, S. Candemir, L. Folio, J. Siegelman, F. M. Callaghan, Z. Xue, K. Palaniappan, R. K.Singh, S. K. Antani, "Automatic tuberculosis screening using chest radiographs", *IEEE Trans Med Imaging,* Vol. 33, No. 2, pp.233-45. 2014.

[27] F. Cao and H. Zhao, "Automatic lung segmentation algorithm on chest X-ray images based on fusion variational autoencoder and three-terminal attention mechanism", *Symmetry,* Vol. 13, No. 5, pp. 814-823, 2021.

[28] M. Kim, B. D. Lee, "Automatic lung segmentation on chest X-rays using self-attention deep neural network", *Sensors,* Vol. 21, No. 2, pp.369-381, 2021.

[29] F. Munawar, S. Azmat, T. Iqbal, "Segmentation of lungs in chest X-Ray image using generative adversarial networks", *IEEE Access,* Vol. 8, pp.153535-153545, 2020.

[30] H. J. Chen, S. J.Ruan, S. W. Huang, "Lung X-ray segmentation using deep convolutional neural networks on contrast-enhanced binarized images", *Mathematics*, Vol. 8, No. 4, pp.545, 2020.

[31] W. Nimalsiri, M. Hennayake, K. Rathnayake, T. D. Ambegoda and D. Meedeniya, "CXLSeg Dataset: Chest X-ray with Lung Segmentation", In: *Proc. of International Conference On Cyber Management And Engineering (CyMaEn)*, Bangkok, Thailand, pp. 327-331, 2023.

[32] A. Singh, M. Sharma and M. Bhattacharya, "Automated Semantic Segmentation of Chest X-ray images using Deep Learning Model", In: *Proc. of IEEE Bombay Section Signature Conference (IBSSC)*, Gwalior, India, pp. 1-6, 2021.

[33] V. Bosdelekidis, N.S. Ioakeimidis, "Lung field segmentation in chest X rays: A deformation-tolerant procedure based on approximating rib cage seed points", *Appl. Sci.* Vol.10, No. 18, pp.6264, 2020.

[34] M. F. Rahman, T. L. B. Tseng, M. Pokojovy, W. Qian, B. Totada, and H. Xu, "An automatic approach to lung region segmentation in chest x-ray images using adapted U-Net architecture", *Medical Imaging 2021: Physics of Medical Imaging*, Vol. 11595, pp. 894-901, 2021.